Automated Tumour Delineation Using Joint PET/CT Information

Vaclav Potesil [1,2], Xiaolei Huang [1,3], Xiang Sean Zhou [1],
[1]Siemens Medical Solutions USA, Computer Aided Diagnosis and Therapy Solutions; [2]Univ. of Oxford (United Kingdom); [3]Lehigh University

ABSTRACT

In this paper, we propose a new method for automated delineation of tumor boundaries in whole-body PET/CT by jointly using information from both PET and diagnostic CT images. Our method takes advantage of initial robust hot spot detection and segmentation performed in PET to provide a conservative tumor structure delineation. Using this estimate as initialization, a model for tumor appearance and shape in corresponding CT structures is learned and the model provides the basis for classifying each voxel to either lesion or background class. This CT classification is then probabilistically integrated with PET classification using the joint likelihood ratio test technique to derive the final delineation. More accurate and reproducible tumor delineation is achieved as a result of such multi-modal tumor delineation, without additional user intervention. The method is particular useful to improve the PET delineation result when there are clear contrast edges in CT between tumor and healthy tissue, and to enable CT segmentation guided by PET when such contrast difference is absent in CT.

Keywords: Tumor delineation, PET-CT, segmentation, radiation therapy planning

1. INTRODUCTION

Fluorodeoxyglucose (FDG)-positron emission tomography (PET) is a whole-body imaging technique that has been recognized as an effective tool for diagnosis, prognosis, staging and response to therapy in oncological imaging. During a FDG-PET scan, a tracer dose of the radioactive material, FDG, is injected intravenously. The FDG uptake is increased in cells with high metabolic rate, hence diseased areas (such as tumor, inflammation) in FDG-PET appear as high-uptake hot spots.

The problem of accurate delineation of tumor boundaries with high reproducibility is essential for radiation therapy in critical regions such as head or volumetric assessment of tumor growth and therapy response. There has been prior work on tumor detection, segmentation, quantitative measurement of tumor volume and change quantification in PET from both clinical study literature [5, 6, 7, 8] and medical image processing literature [10, 11]. Most approaches use the standard uptake value (SUV), which is a semi-quantitative normalization of the FDG uptake in PET images and measures the FDG concentration normalized by decay corrected injection dose per gram body mass. Physicians and radiologists have used this measure for normalization across time points and across different patients, and the maximum SUV values are used for grading tumors. Typically hot spots are detected as local regions with high SUV values, and segmentation algorithms apply thresholds that relate to the maximum SUV value. However, precise delineation of the hot spot boundary from PET alone remains challenging, because intensity decreases smoothly and gradually from the hot spot core to normal tissue and there is no sharp contrast separating diseased and healthy tissue. There are also the issues with intrinsic imaging pitfalls and artifacts in PET [10, 14] and the lack of ground truth for validating proposed algorithms.

The PET/CT technology combines functional PET and anatomical CT scanning technologies and allows the acquisition of clinical quality PET and CT scans, accurately aligned, from a single imaging device [13]. On the fused PET/CT image, abnormalities that are seen on PET can be located, and possibly also confirmed, on CT, and this enables the interpreting physician to make a more informed decision about whether the hot spot on PET is indeed an abnormality, and if so, where the abnormality is located anatomically. Retrospective studies performed with PET/CT prototypes showed considerable promise, particularly in the areas of disease staging and therapy planning and monitoring.

Previous works on PET/CT image analysis, change quantification, and visualization [15, 16] have mostly focused on registration and fusion to compensate for movements/deformations due to patient positioning, physiological organ motion, or structural changes as a result of disease progression or remission. These registration methods have demonstrated success in correcting organ (such as breast, lung, liver) motion. There is little work on utilizing PET/CT information to improve segmentation (e.g. tumor boundary delineation) accuracy. CT provides higher spatial resolution compared to PET, however automated segmentation algorithms often fail when used on CT data alone because the attenuation difference between tumor and surrounding health tissue is often too low to show clear contrast edges in CT. On the other hand, the gradual change of intensity in PET images makes it difficult to delineate tumor boundary precisely using PET alone.

In this paper, we propose a new method for automated delineation of tumor boundaries in whole-body PET/CT by jointly using information from both PET and diagnostic CT images. The method exploits complementary information from PET and CT, improving the PET delineation result when there are clear contrast edges in CT, and enabling CT segmentation guided by PET when contrast difference is absent in CT. Combining the high-sensitivity for detection of cancerous tissue in PET and superior spatial resolution of complementary diagnostic CT images, we show that efficient, robust and reproducible segmentation can be achieved with minimal user interaction, assuming ideal registration of PET/CT.

2. METHOD

Our method has two major components based on our recent research: (1) the one-click tumor delineation algorithm for whole-body PET based on mode-seeking region growing [1] for robust and reproducible tumor delineation in PET, and (2) CT segmentation based on intensity likelihood ratio test [2]. The method takes advantage of an initial robust segmentation performed in PET, to learn a model for tumor appearance and shape in corresponding CT structures. More accurate and reproducible tumor delineation can be achieved as a result of such multi-modal tumor delineation, without additional user intervention. The algorithm consists of the following main steps.

2.1. Lesion detection and robust lesion segmentation in PET

A region with high FDG uptake is initially detected in PET by the physician or using an automated hot-spot detection algorithm [1].

This region may potentially include several local hot spots. In order to obtain a reliable initial segmentation of hot spots, we apply a *Mode-Seeking Region Growing* segmentation algorithm (MSRG) . Mode-seeking is the process of finding voxel locations with local maximum SUV values (SUV_{max}) within the region of interest. In this step, we start from each seed point as a probe on the 4-D surface as defined by the spatial coordinates *(x,y,z)* and the corresponding SUV intensity $I_{SUV}(x,y,z)$. At the probe point, we find the maximum SUV value within its local neighbourhood and then move the probe to the point with that maximum. The process continues until the probe reaches the intensity mode in the given region of interest. By starting the mode-seeking procedure from many seed points uniformly distributed within a VOI, we can detect all the SUV-maxima points that correspond to the primary locations of true hot spots. SUV images tend to be locally smooth, which facilitates the mode-seeking processes even with a relatively low number of seed points.

Next we apply 3D region growing, originated from the detected local modes, with a fixed threshold of 40% of the corresponding SUV_{max} value. This produces a conservative segmented lesion mask in PET, based on a clinically meaningful threshold that has been utilized in the literature[7]. Radiologists commonly use the maximum SUV value of a tumour candidate in order to grade the disease and help determine its spatial extent [6, 8, 9]. Hence, the segmentation based on maximum local SUV value produces results consistent with the clinically used criteria. Overall the mode-seeking region growing method has been validated extensively and it produces accurate, reproducible results that are not sensitive to the seed point.

2.2. Modeling tumor appearance in CT by weighted non-parametric density estimate

Let us denote the segmented hot spot areas by mode-seeking region growing as VOI_{in}. We consider VOI_{in} only containing lesion tissue because of the conservative 40% of SUV_{max} threshold. We then obtain another volume of interest , $VOI_{out,}$ which is considered to contain only non-lesion tissue, by first dilating generously the original mask VOI_{in} using a 3D structuring element and then excluding VOI_{in} from the dilated mask. Morphological operations are restricted to respect other pre-segmented structures, including body outline, heart and other detected hotspots.

A probabilistic model of tissue attenuation in CT in both the segmented tumor (i.e. lesion) as well as in the background (i.e. non-lesion) can be obtained in terms of CT intensity likelihood functions using weighted non-parametric density estimates. Let the CT value, $I_{CT}(x)$, at a voxel, x, be α, then we can approximate the likelihood of this intensity, in a lesion, or outside a lesion by:

$$f(\alpha \mid in) = \frac{1}{|V|} \int_{y \in VOI_{in}} g(I_{SUV}(y) \mid in)\, K_{\sigma}(I_{CT}(y) - \alpha)\, dy, \qquad (1)$$

$$f(\alpha \mid out) = \frac{1}{|V|} \int_{y \in VOI_{out}} g(I_{SUV}(y) \mid out)\, K_{\sigma}(I_{CT}(y) - \alpha)\, dy, \qquad (2)$$

Where α refers to CT intensity value, K_{σ} is a 3-dimensional kernel function with bandwidth σ, VOI_{in} and VOI_{out} are spatial supports based on PET lesion segmentation, V is a volume normalization factor. $g(I_{SUV}(y) \mid in)$, $g(I_{SUV}(y) \mid out)$ model the likelihood of tumor appearance at voxel y in PET, and they are defined by:

$$g(I_{SUV}(y) \mid in) = \frac{1}{1 + e^{-\beta((I_{SUV}(y)+\tau)*\upsilon - \psi)}}, \qquad (3)$$

$$g(I_{SUV}(y) \mid out) = 1 - g(I_{SUV}(y) \mid in), \qquad (4)$$

where β is a parameter defining the extent of CT density estimates weighting (determined empirically for a given clinical application and fixed, in our test cases $\beta = 0.4$), $I_{SUV}(y)$ is the SUV intensity at voxel y normalized to [0,1] and τ, υ, ψ scale and center the sigmoid function so that $g(40\% SUV_{\max} \mid in) = 0.5$. The function is adjusted accordingly if a different threshold was used to obtain PET segmentation.

2.3. Joint Likelihood Ratio Test

A joint-likelihood ratio $r(x)$ is calculated on a voxel-by-voxel basis in the joint PET-CT domain to provide a measure of voxel being containing lesion tissue as opposed to being in background, assuming PET and CT are independent given the ground truth classification for *in* and *out*.

$$r(x) = \frac{L(in \mid (x, I_{CT}, I_{SUV}))}{L(out \mid (x, I_{CT}, I_{SUV}))} \propto \frac{L(x, I_{CT} \mid in) L(x, I_{SUV} \mid in)}{L(x, I_{CT} \mid out) L(x, I_{CT} \mid out)} = \frac{f(I_{CT}(x) \mid in) g(I_{SUV}(x) \mid in)}{f(I_{CT}(x) \mid out) g(I_{SUV}(x) \mid out)}, \qquad (5)$$

In the Eq. (5) above, the likelihood functions, L , are defined based on f and g likelihoods in Eqs. (1)~(4), and are evaluated on an isotropic grid using linear interpolation of CT and SUV intensity values. Tumor-background

membership is determined by binary classification of each voxel to be within either VOI_{in} or VOI_{out} using the likelihood ratio test[2], which is basically a thresholding operation on *r(x)* using the threshold *1.0*. The likelihood ratio test and class membership assignment are repeated for a fixed number of iterations to reach a stable value (in our case, n=3 was determined empirically as a suitable parameter).

If PET is only used for hot-spot detection and producing the initial volume estimate for tumor foreground and background appearance modeling in CT, the previous equation simplifies as

$$r(x) = \frac{L(in \mid (x, I_{CT})}{L(out \mid (x, I_{CT})} \qquad (6)$$

Optionally, to prevent the segmentation result on CT from flooding away in case of adjacent structures having identical attenuation, a constraint on segmented tumor shape can be imposed in terms of a Gaussian spatial likelihood function as in [4]. The center, scale and anisotropy of the Gaussian are determined from VOI_{in}.

3. DATA

We have tested the algorithm on multiple patient studies with lung and liver tumors identifiable in both the PET scan and the corresponding diagnostic CT scan acquired using the same scanner. In some datasets a difference in respiration protocol between PET, CT resulted in spatial mismatch between PET and CT tumor centre locations. These images were then semi-automatically registered.

The lung cancer datasets included four patients with a total of six tumors of different shapes. The liver cancer datasets included one patient with three liver tumors and there are three independent studies acquired several months apart for this patient.

4. RESULTS

The system has produced robust results on segmenting liver and lung tumors in multiple patients based on PET and diagnostic CT scans. The expert ground truth segmentation was not available for the studied cases and therefore we performed a qualitative assessment.

4.1. Liver tumors

Tumour boundaries are visible on CT but cannot be reliably segmented using CT data alone [2] due to low intensity gradient in the tumour boundaries. In PET, the segmentation is affected by high natural FDG uptake in liver. Our joint PET/CT algorithm with conservative initial threshold gives good segmentation of tumors located in high-activity regions, which cannot be segmented automatically by using PET alone.

Figure 1 shows example segmentation results for various lesions of hepatocellular carcinoma. The segmentation worked well for varying maximum SUV_{max} in the tumours in images acquired at 3 time points at different stages of disease development. Joint PET-CT segmentation enabled more accurate apparent localization of tumour boundaries and volume and can provide valid segmentation even if the default PET segmentation threshold (40%) fails due to high activity in neighboring regions.

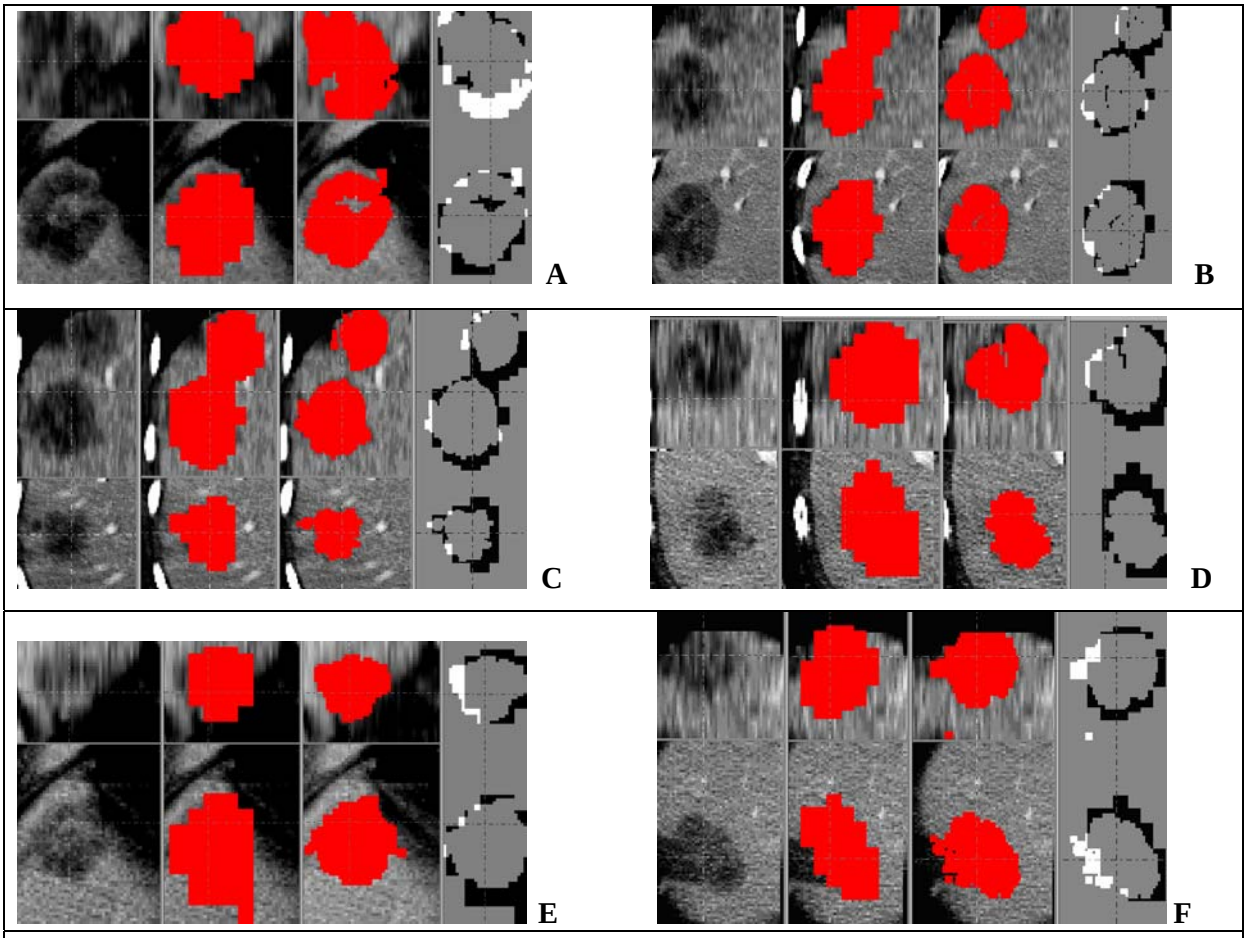

Figure 1 From left: liver lesion in CT image (1), PET-only result (2), new PET-CT algorithm result (3), binary difference image defined as 3-2 (4). Top row: coronal plane, bottom: axial plane.

Along the boundaries of liver tumors shown in Figure 1, the intensity gradients are very low compared to gradients separating other structures in the image, as can be seen from Figure 2. Therefore, many methods based on CT intensity alone will fail.

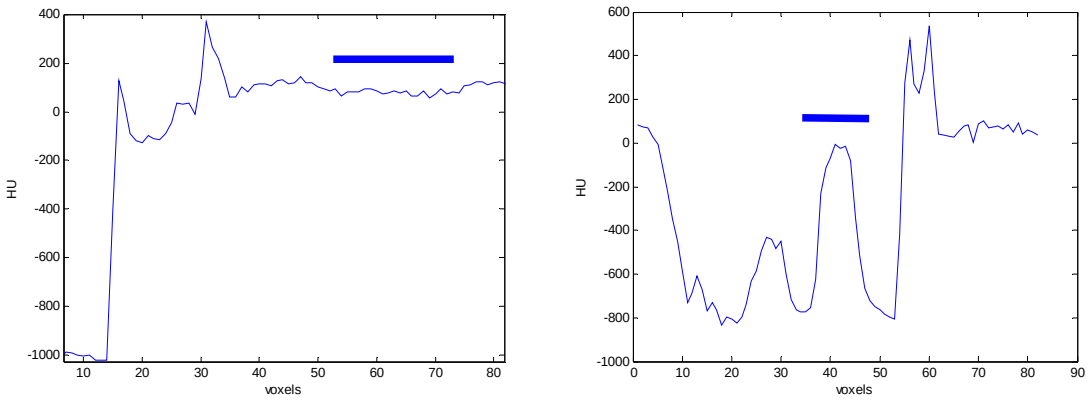

Figure 2 The intensity profiles of liver tumor (Figure 1 A) and lung tumour (Figure 3 A) along the horizontal line of the cursor. The highlighting in the intensity profile indicates the location of the tumour.

Figure 3 shows small malignant lung nodules distally located (A, B, C, F) and near mediastinum (B, E). PET-CT algorithm provides better delineation of tumour boundaries than PET region growing segmentation that suffers from insufficient resolution. CT-only algorithm may be negatively affected by other structures with similar attenuation, such as vessels, airways, lung wall, and others. Spatially co-registered PET and CT data are assumed.

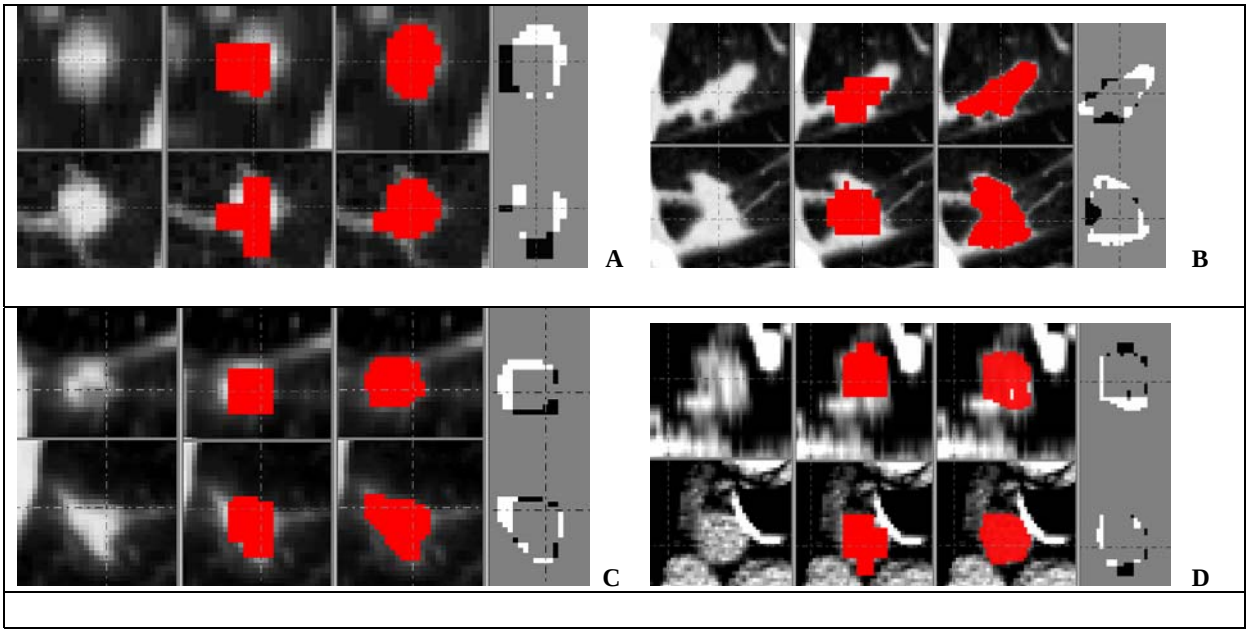

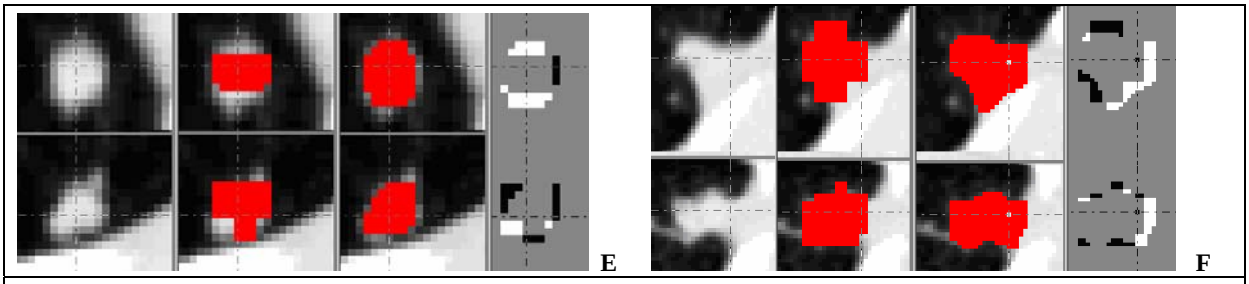

Figure 3 From left: lung lesion in CT image (1), PET only result (2), new PET-CT algorithm result (3), binary difference image defined as 3-2 (4). Top row: coronal plane, bottom: axial plane.

5. CONCLUSIONS

Integration of PET and CT segmentation enables automated tumor delineation when PET-only based methods fail, such as in the case of tumors located in liver or proximity of structures with high normal FDG uptake. PET provides robust detection and a conservative tumor structure delineation, used as an initialization for CT segmentation. CT intensity models learned on lesion and background then provide the basis for testing the class of each voxel, and the classification is probabilistically integrated with PET classification to derive the final improved result. The algorithm requires minimal user interaction and proves the potential of combining PET and CT information for robust and accurate tumor segmentation. More sophisticated PET/CT information integration algorithms are under investigation and the outcome will eventually be included as a part of a segmentation toolbox within computer-aided diagnosis software developed by Siemens Medical Solutions.

6. REFERENCES

[1] H. Guan, T. Kubota, X. Huang, X. Zhou, M. Turk. *Automatic Hot Spot Detection and Segmentation in Whole Body FDG-PET Images*. In Proc. of the IEEE Int'l Conf. on Image Processing (ICIP), 2006.

[2] K. Okada, U. Akdemir, A. Krishnan. *Blob Segmentation using Joint Space-Intensity Likelihood Ratio Test: Application to 3D Tumor Segmentation.* In Proc. of the IEEE Computer Society Conf. on Computer Vision and Pattern Recognition (CVPR), Vol. 2, pp. 437-444, 2005.

[3] U. Nestle, S. Kremp, A. Schaefer-Schuler, C. Sebastian-Welsch, D. Hellwig, C. Rube, and C. M. Kirsch. *Comparison of Different Methods for Delineation of ^{18}F-FDG PET – Positive Tissue for Target Volume Definition in Radiotherapy of Patients with Non-small Cell Lung Cancer.* J. of Nuclear Medicine, 46(8):1342-1348, 2005.

[4] K. Okada, D. Comaniciu, A. Krishnan. *Robust Anisotropic Gaussian Fitting for Volumetric Characterization of Pulmonary Nodules in Multislice CT.* IEEE Trans. on Medical Imaging, 24(3):409-423, 2005.

[5] J. F. Daisne, T. Duprez, B. Weynand, M. Lonneux, M. Hamoir, H. Reychler, V. Gregoire. *Tumor Volume in Pharyngolaryngeal Squamous Cell Carcinoma: Comparison at CT, MR Imaging, and FDG PET and Validation with Surgical Specimen.* Radiology, 233(1):93-100, 2004.

[6] N. Khan, N. Oriuchi, A. Yoshizaki, T. Kanuma, T. Kiguchi, and K. Endo. *Diagnostic Accuracy of FDG PET Imaging for the Detection of Recurrent or Metastatic Gynecologic Cancer.* Annals of Nuclear Medicine, 19(2):137-145, 2005.

[7] Q. C. Black, I. S. Grills, L. L. Kestin, C. Y. O. Wong, J. W. Wong, A. A. Martinez, D. Yan. *Defining a Radiotherapy Target with Positron Emission Tomography.* Int. J. Radiation Oncology Biol. Phys., 60(4):1272-1282, 2004.

[8] T. R. Miller, P. W. Grigsby. *Measurement of Tumor Volume by PET to Evaluate Prognosis in Patients with Advanced Cervical Cancer Treated by Radiation Therapy.* Int. J. Radiation Oncology Biol. Phys., 53(2):353-359, 2002.

[9] P. D. Shreve, Y. Anzai, and R. L. Wahl. *Pitfalls in Oncologic Diagnosis with FDG PET Imaging: Physiologic and Benign Variants.* Radiographics, 19(1):61-77, 1999.

[10] D. Jakobsson, F. Olofsson. *Decision Support System for Lung Cancer using PET/CT Images.* Master Thesis, Centre for Mathematical Sciences, Lund Institute of Technology, Lund University, Lund, Sweden.

[11] M. Lysaker, T. F. Chan, X. C. Tai. *Level Set Method for Positron Emission Tomography.* UCLA CAM-report 04-30, 2004. Electronic version at http://www.mi.uib.no/BBG/papers/LysakerChanTai.pdf

[12] M. Ivanovic, S. Loncaric, W. H. McCartney, A. Khandani. *Evaluation of PET Standard Uptake Value's Dependence on Imaging Protocols for Dual Time Point Imaging.* Nuclear Science Symposium Conference Record, IEEE, Vol. 7, pages 4076-4079, 2004.

[13] D. W. Townsend, T. Beyer, T. M. Blodgett. *PET/CT Scanners: A Hardware Approach to Image Fusion.* Seminars in Nuclear Medicine, Vol.xxxiii, No. 3, pp. 193-204, 2003.

[14] G. K. Von Schulthess. *Normal PET and PET/CT Body Scans: Imaging Pitfalls and Artifacts.* Ch. 39, Clinical Molecular Anatomic Imaging: PET, PET/CT and SPECT/CT, Lippincott Williams & Wilkins publishers, 2003.

[15] C. Behrenbruch, K. Marias, P. Armitage, M. Yam, N. Moore, R. English, J. Clarke, and M. Brady, *Fusion of contrast-enhanced breast MR and mammographic imaging data,* Medical Image Analysis, 7: 311-340 (2003).

[16] K. Marias, C. Behrenbruch, S. Parbhoo, A. Seifalian, M. Brady. *A Registration Framework for the Comparison of Mammogram Sequences.* IEEE. Trans. Medical Imaging, 24(6):782-790, 2005.